Orbital Constraints on Exoplanet Habitability

Zachery McBrearty

Level 4 Project, MPhys Physics with Astronomy

Supervisor: Dr Richard Wilman

Second Supervisor: Dr Craig Testrow

Department of Physics, Durham University

Submitted: March 14, 2024

A 1-D energy balance climate model is developed in order to investigate how changing certain orbital parameters can result in changes to a planet's habitability. Theoretical relationships between temperature, semimajoraxis, and eccentricity are derived from a 0-D energy balance model and are tested against the 1-D model and are found to be correct. A qualitative analysis of obliquity shows that there are optimal obliquities to minimise and maximise global temperature. The climates of exomoons orbiting gas giants are also investigated, including reflected light from the gas giant, eclipsing, and tidal heating. It is expected that these additional sources of heat move the habitable zones for the planet outwards.

CONTENTS

1.   INTRODUCTION

A.   Exoplanet and Exomoon detection

When the first exoplanet was discovered is up for debate depending on classification [1]. To give a summary: The first evidence for an exoplanet came in 1988 but was attributed to stellar activity. This was followed up later in 2003 and found to be a exoplanet. This confirmation happened many years after 1992 when the first exoplanets were found orbiting a pulsar via the variations in pulsar timings due to those exoplanets. However the intensity of radiation from these pulsars make life on these exoplanets impossible. Then the first potentially habitable exoplants were found in 1995; potentially habitable because they orbit a Sun-like star.

Exoplanets are now found in a variety of indirect and direct methods. Indirect methods include pulsar timing, radial velocity, astrometry, and gravitational lensing. Direct methods include transits and direct imaging via coronagraph. Direct and indirect methods have also been combined to find planets. For example Kepler-88c was discovered indirectly due to variation in the transit of Kepler-88b [2].

These methods can also be extended to find exomoons around exoplanets. The pulsar timing from an exoplanet has additional variations due to a exomoon [3] and it has been shown that nearby exomoons may be found using Kepler (or Kelper-class) photometry by analysing variations in transit timing signals [4].

More recently, it has been shown that exomoons with strong tidal heating could be brighter brighter than the exoplanet they orbit, so are easier to detect than exoplanets in some cases [5]. Further, the launch of the JWST has enabled the direct detection of earth-sized exomoons with economical use of observation time [6].

The culmination of all these methods is collated by the Encyclopaedia of Exoplanetary Systems [7] who report a total of 5641 exoplanets confirmed but no exomoons.

Reaching these exoplanets is a project for the far future, however current missions are building up to this auspicious goal. The one recent (and on going) mission is the Artemis Plan [8] which plans to build a Base Camp on the lunar surface and setup Gateway in lunar orbit. Additionally, the China National Space Administration also plan to return to the moon with the International Lunar Research Station [9]. Both these projects will allow for human settlement away from the Earth, and are vital in progressing further out into our own solar system and beyond.

B.   Energy balance models

Analysing the habitability of exoplanets can be difficult. The Trappist-1 system is an excellent example. In the system seven Earth-like planets were found within the habitable zone of their host star [10]. However they are not habitable due to a mixture of being tidally-locked to the star and experiencing extreme solar winds which have probably stripped them of any atmosphere long ago [11, 12]. This suggests that modelling of an exoplanet's habitability requires modelling of the dynamic atmosphere,

One way to model the exoplanets is with an energy balance model, where incoming energy

(usually from a star) is equated to outgoing energy (usually blackbody emission). If no time dependence is considered then the 0-D Energy Balance Model (0DEBM) is

$$\pi r^2 S(1 - A) = 4\pi r^2 \sigma T^4, \tag{1}$$

where r is the radius of the planet, S is the incoming solar radiation (insolation) which is reduced by the albedo of the planet A. The blackbody term is given by the Stefan-Boltzmann constant, σ, and the temperature of the planet T. This model does not resolve the planet's surface, and comes with a variety of assumptions such as energy being distributed equally over the entire planet's surface. This assumption implies that the planet is not tidally locked and has good diffusion mechanisms to spread out heat.

While this 0DEBM is powerful, there are limitations. The temperature produced is an average over time which means extreme temperatures are ignored. Additionally, different latitude bands experience different amounts of insolation depending on time and obliquity, thus the assumption of even energy distribution is not entirely valid. This is especially apparent on the Earth where the poles have much lower temperatures (i.e. freezing) compared to the equator.

These problems can be addressed with a 1-D Energy Balance Climate Model (1DEBCM). The 1DEBCM is given in latitude, λ, and time, t, coordinates as

$$C(\lambda, T)\frac{\partial T(t, \lambda)}{\partial t} = D\left[\frac{\partial^2 T(t, \lambda)}{\partial \lambda^2} - \tan\lambda\frac{\partial T(t, \lambda)}{\partial \lambda}\right] + S(\lambda, t)(1 - A(T)) - I(T), \tag{2}$$

where C is the heat capacity for a latitude band, D is the diffusion constant regulating the horizontal transport of heat between latitude bands, I is the generalised IR emission for a latitude band. The other terms are the same as the 0DEBM. Specific forms for these functions for the Earth-like model are given in Section 2 A. This model still assumes that the planet is not tidally locked, and that the insolation received is thus an average over a day (diurnally averaged) which is spread over the entire latitude band. The assumption that all latitudes are the same temperature is lifted compared to the 0DEBM.

The 1DEBCM can be derived from the heat equation (see Section 2) and was originally developed by North and Coakley 1979 (NC79) [13] to study the Earth. It was then further applied by Williams and Kasting 1997 (WK97) [14] to study obliquity dependent habitability and then by Spiegel et al in 2008 (SMS08) [15] and 2009 [16] to study quantify habitability and then study obliquity dependent habitability. Spiegel's work was furthered by Dressing et al 2010 (Dressing10) [17] where eccentricity dependent habitability was investigated. This paper investigates the effects of varying semimajor axis and eccentricity on habitability (Sec. 3 A), as well as obliquity dependence of habitability (Sec. 3 B), and the minimum ratio of ocean to land for the planet to prevent ice-albedo-feedback (Sec. 3 C).

An aspect of the 1DEBCM which is not present in the 0DEBM is ice-albedo-feedback (IAB). It is not present in the 0DEBM because the albedo is constant and the model is not dynamic.

In the 1DEBCM, albedo is a function of temperature where lower temperatures have high albedo and high temperatures have low albedo. If temperature decreases, more ice forms thus albedo increases. This increased albedo means more insolation is reflected, thus the model has even less input heat and so cools further and forms more ice.

Thus IAB is positive feedback loop between ice formation and albedo which can result in a 'snowball' model which is entirely covered in ice. The susceptibility of the model to IAB can

be estimated using the thermal timescale,

$$\tau = \frac{CT}{I},\tag{3}$$

which is the energy in the model divided by the speed of removal of that heat via IR emission. This definition suggests that a larger heat capacity requires a longer time period to change, thus should be less susceptible to IAB.

This is reflected in Sec. 3 C where ocean fraction (thus heat capacity) in the model is varied, and it is found that low ocean fraction (low heat capacity) is much more susceptible to IAB due to the smaller thermal timescale. Two main sources of reduced temperatures are investigated. The first source is eccentricity, where IAB can happen if the planet spends a long time away from the star and cools to a snowball state. The second is obliquity, where IAB can freeze the pole which is facing away from the Sun and then reflect enough light when facing the Sun to allow the entire model to fall into a snowball state.

It is found that obliquity requires higher minimum ocean fraction than eccentricity to avoid IAB and falling into a snowball state, thus is a more powerful constraint on the habitability if the ocean fraction of an exoplanet is known. The disadvantage of this is the eccentricity of the orbit is much easier to observe than the obliquity of the planet relative to the star it orbits.

The 1DEBCM must be validated against known data. To do this a similar process to the one WK97 use to calibrate their model is followed. NC79 used data from various sources and developed a model using Legendre polynomials for latitude variation and sine and cosine functions for time variation. The first 3 terms of the global temperature model are given in their eqn. (4) as

$$T(\lambda, t)[°\text{C}] = 14.2 + 15.5\cos(\omega t + \phi)P_1(\sin\lambda) - 30.2P_2(\sin(\lambda)),\tag{4}$$

where P_i is the ith Legendre polynomial. Taking the time-average of this function over a year period gives

$$\begin{aligned}
T(\lambda)[\text{K}] &= 14.2 + 273 - 30.2(3\sin^2(\lambda) - 1)/2 \\
&= 302.3 - 45.3\sin^2(\lambda),
\end{aligned}\tag{5}$$

where the temperature has been converted to Kelvin, and the second legrendre polynomial is expanded as $P_2(x) = (3x^2 - 1)/2$. The average of $\cos(\omega t + \phi)$ over an period $T = 2\pi/\omega$ is 0, so the first legendre polynomial is not needed. This time-averaged model is then used to fix the diffusion D for the model in Section 2 A.

C. Habitability

Once the model has been run for a particular set of variables, lots of temperature data for time and latitude must then be processed to evaluate the habitability of the model.

The two habitability functions used in this paper are Liquid Water Requirement (LWR) and Human Compatible (HC). LWR is the more familiar of the two where a temperature between the melting point and boiling point of water is habitable, functionally given as

$$H_{\text{LWR}}(T) = \begin{cases} 1 & 0°\text{C} \leq T \leq 100°\text{C} \\ 0 & \text{Otherwise.} \end{cases}\tag{6}$$

The alternatively, the HC habitability is defined with a smaller range of values,

$$H_{\text{HC}}(T) = \begin{cases} 1 & 0°\text{C} \leq T \leq 30°\text{C} \\ 0 & \text{Otherwise,} \end{cases} \tag{7}$$

with the additional stipulation that if a latitude band experiences a temperature greater than $40°$C or less than $-10°$C then the band is considered uninhabitable for all time. The motivation for this temperature range and restriction of extreme temperatures comes from the ability for humans to self regulate their internal temperature. The typical temperature used to assess human survivability is a wet bulb temperature of $T_w = 30°$C. However this value can underestimate the onset of hyperthermia and overestimate lethality [18]. This motivates the underestimate of habitability decreasing at $30°$C and being lethal at the higher $40°$C. The minimum temperature is simply a symmetry of the maximum case, and is less important due to cold places staying cold due to IAB.

SMS08 quantifies habitability in 3 main ways. The first is the time-averaged habitability, f_{time}, which is given in their eqn. (6) as

$$f_{\text{time}}(q, \lambda) = \frac{1}{P} \int_0^P H(q, \lambda, t) dt, \tag{8}$$

where P is the length of the year for the model in question and $H(q, \lambda, t)$ is a habitability function; 1 if the temperature is habitable, 0 if not. The second is the area-weighted habitability, f_{area}, which is given in their eqn. (7) as

$$f_{\text{area}}(q, t) = \frac{1}{2} \int_{-\pi/2}^{\pi/2} H(q, \lambda, t) \cos(\lambda) d\lambda, \tag{9}$$

where the area weighting occurs as each latitude band has unequal area. Finally the combination of these two measures results in the total habitability, f_{total}, given in their eqn. (8) as

$$f_{\text{total}}(q) = \frac{1}{2P} \int_{-\pi/2}^{\pi/2} \int_0^P H(q, \lambda, t) dt \cos(\lambda) d\lambda, \tag{10}$$

where in all three cases the semimajor axis a has been replaced by a generalised parameter (or set of parameters) q. This paper uses the discrete form of these equations in Section 2 C in order to both quantify when a model has reached an stable average (i.e. equilibrium) temperature and for quantifying the habitability of a model which varies in time and latitude.

D.   Modifications for Exomoons

In this paper the moon is an Earth-sized moon and the planet is a Jupiter-sized gas giant. In our own solar system there are no moons which come close the size of the Earth, which presents the question: do Earth-sized exomoons exist? The answer is in two parts. First, mass $m > 0.12 M_{\text{Earth}}$ and a strong magnetic field [19] would be required for a "substaintial and long-lived atmosphere", thus the exomoons must be high mass. Second, mechanisms such as binary capture [20] can allow for high mass moons where the usual accretion models, such as those that formed the moons seen in the outer solar system, do not.

In order to investigate exomoons the 1DEBCM must be modified to include three heat sources and a reduction to insolation.

In section 4 A eclipsing is investigated and quantified into an eclipsing fraction ϵ. This eclipsing fraction is added to the model as a reduction to the insolation,

$$S(1 - A) \rightarrow S(1 - A)(1 - \epsilon), \tag{11}$$

In section 4 B the flux received from the moon due to light from the sun being reflected by the gas giant as well as the emission of light from the gas giant are quantified and added to the model as F_{ref} and F_{emiss} respectively. The reflected light from the gas giant is supposed to be from the light not absorbed by the gas giant, which is just the incident light from the sun times the albedo of the gas giant. The emission of the light from the gas giant is then emission of a blackbody in equilibrium given by the 0DEBM. The moon model assumes that the gas giant has radiated all of it's heat of formation and thus is in thermal equilibrium with the sun. This is not the case for Jupiter in our own solar system, which the model bases the gas giant after [21], but the additional heat is small.

In section 4 C the tidal heating of the moon due to it's elliptical orbit around the gas giant is quantified. Tidal heating equations are described in detail for the specific case of Io in [22, 23] and for general exoplanets in [24, 25]. The general equation for tidal heating is given by

$$F_{\text{th}} = -\frac{21}{8\pi}\text{Im}(k_2)\frac{G^{3/2}M_{\text{gas}}^{5/2}R_{\text{moon}}^3 e_{\text{moon}}^2}{a_{\text{moon}}^{15/2}}, \tag{12}$$

where the mass, radius, eccentricity, and semimajor axis of the subscripted body are given by M, R, e, and a respectively. Specific values for $-\text{Im}(k_2)$ are derived from different rheologies and material compositions of the moon. In this paper the Maxwell rheology from Henning et al [26] is used as well as the material compositions from Dobos and Turner [24].

Thus the moon model is, with all modifications made, given by

$$\begin{aligned}
C\frac{\partial T}{\partial t} =& D\left[\frac{\partial^2 T}{\partial \lambda^2} - \tan\lambda\frac{\partial T}{\partial \lambda}\right] - I(T) \\
& + F_{\text{ref}} + F_{\text{emiss}} + F_{\text{th}} + S(1 - A_{\text{moon}})(1 - \epsilon).
\end{aligned} \tag{13}$$

With this moon model the habitable zones investigated in Sec. 3 can be revisited to see how they are affected by the changes (Sec. 4 D). New habitable zones also emerge depending on the moon's parameters. The semimajor axis and eccentricity of the moon's orbit are investigated in Sec. 4 E.

2.   1-D ENERGY BALANCE CLIMATE MODEL

The 1DEBCM can be derived from the standard heat equation given by

$$\frac{\partial T}{\partial t} = \alpha\nabla^2 T, \tag{14}$$

where $T(t, r, \theta, \phi)$ is the temperature at time t, radius r, co-latitude θ, and longitude ϕ. The constant α is related to the heat capacity and diffusion rate of the system. Expanding the laplacian

Semimajoraxis a, au	Eccentricity e	Obliquity δ, deg	No. spatial nodes S	Timestep Δt, days	Land fraction type
1	0.0167	23.5	61	1	Uniform 70% Ocean

TABLE I: A summary of the default parameters for the Earth-like model. A 'Uniform' land fraction indicates that the model has the same ratio of land to ocean across the entire planet. The odd number of spatial nodes means there is a true equator with $\lambda = 0$ as well as poles with $\lambda = \pm 90°$

in spherical coordinates the equation becomes

$$\frac{\partial T}{\partial t} = \alpha \left[\frac{1}{r}\frac{\partial^2}{\partial r^2}(rT) + \frac{1}{r^2 \sin\theta}\frac{\partial}{\partial\theta}\left(\sin\theta\frac{\partial T}{\partial\theta}\right) + \frac{1}{r^2 \sin^2\theta}\frac{\partial^2 T}{\partial\theta^2} \right]. \tag{15}$$

The 1DEBCM is arrived at by first letting $T(t, r, \theta, \phi) = T(t, \lambda)$, with latitude $\lambda = \pi - \theta$. Thus the equation simplifies to

$$\begin{aligned}
\frac{\partial T}{\partial t} &= \frac{\alpha}{r^2 \sin\theta}\frac{\partial}{\partial\theta}\left(\sin\theta\frac{\partial T}{\partial\theta}\right) \\
&= \frac{\alpha}{r^2}\left(\frac{\partial^2 T}{\partial\lambda^2} - \tan\lambda\frac{\partial T}{\partial\lambda}\right).
\end{aligned} \tag{16}$$

The original equation can be recovered by defining $\alpha/r^2 \equiv D/C$ for diffusion constant D and heat capacity C. Then adding incoming solar radiation S (insolation), which is reduced by planetary albedo A, and outgoing IR-emission I to the PDE. Thus the original form of the 1D EBCM in eqn. (2) is recovered.

A. Earth-like model functions

In order to investigate the Earth and Earth-like planets, the parameters and functions which define the Earth must be established. In this analysis the forms of the Earth-like functions are taken from WK97, and the Earth-like model is compared against a model derived from NC79.

The diffusion constant, D, varies with orbital and atmospheric parameters as

$$\frac{D}{D_0} = \frac{p}{p_0}\frac{c_p}{c_{p,0}}\left(\frac{m}{28}\right)^{-2}\left(\frac{\Omega}{1 \text{ day}^{-1}}\right)^{-2}, \tag{17}$$

where $D_0 = 0.56$ Wm^{-2}K^{-1} is from fitting to eqn. (5) as shown in Fig. 1. The atmospheric pressure, p, is relative to one atmosphere of pressure, $p_0 = 101$ kPa. The heat capacity, c_p, of the atmosphere is relative to $c_{p,0} = 1 \times 10^3$ g^{-1}K^{-1}, which is the heat capacity of nitrogen gas. Average mass of particles in the atmosphere is given by m and is relative to the nitrogen molecule. Rotation rate of the planet, Ω, is relative to Earth's 1 rotation per day. These parameters can be extended to be time variable, such as having CO_2 emissions increase pressure, change heat capacity, and change mass of particles. However this is beyond the scope of this paper.

Heat capacity, $C(\lambda, T)$, varies with latitude through the ocean-land fraction, $f_o(\lambda)$, and with temperature through the ice-ocean fraction, $f_i(T)$, as

$$C(\lambda, T) = (1 - f_o(\lambda))C_{\text{land}} + f_o(\lambda)((1 - f_i(T))C_{\text{ocean}} + f_i(T)C_{\text{ice}}(T)), \tag{18}$$
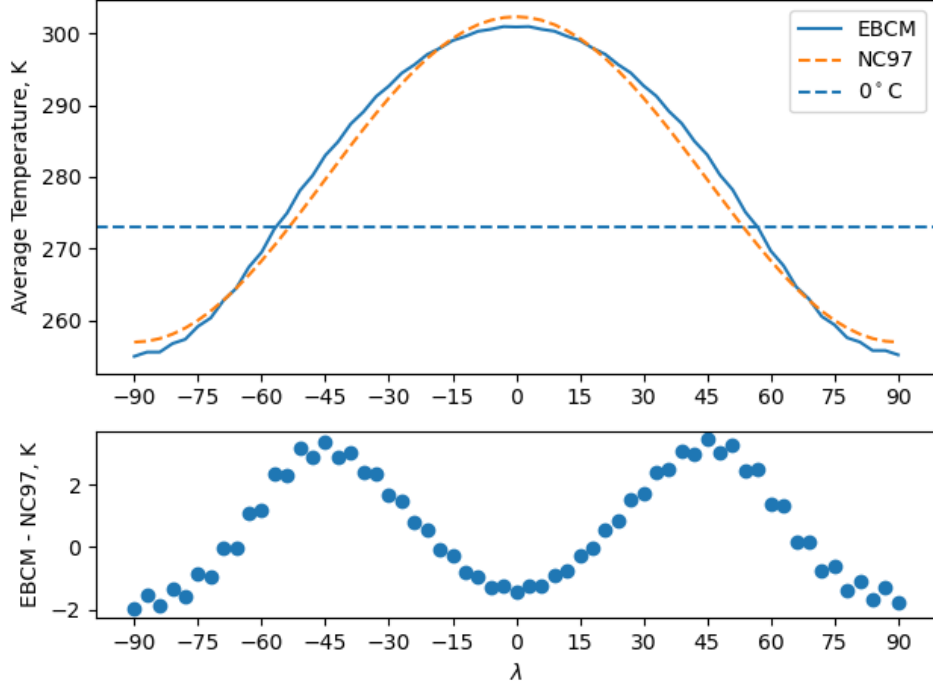
FIG. 1: The 10-year-averaged temperature distribution of the Earth-like model given in I. Overlaid on the fit is the time averaged Earth model from North and Coakley's 1979 paper [13]. The diffusion parameter D_0 in eqn. (17) was varied to give the best agreement between the two models. The value found to work best is $D_0 = 0.56 \, \text{Wm}^{-2}\text{K}^{-1}$.

Where $C_{\text{land}} = 5.25 \times 10^6 \, \text{Jm}^{-2}\text{K}^{-1}$ and $C_{\text{ocean}} = 40 \times C_{\text{land}}$ are constant, and

$$C_{\text{ice}}(T) = \begin{cases} 9.2 C_{\text{land}} & T \geq 263\text{K} \\ 2.0 C_{\text{land}} & T < 263\text{K}, \end{cases} \tag{19}$$

which encapsulates the additional energy requirements of the heat of fusion, and expects that the water would be entirely frozen below $-10°$C. The ratio of ocean to land for the Earth is 70% ocean to 30% land. This model assumes this ratio is uniform and constant across the entire planet, thus $f_o = 0.7$. This is a simplification as the Earth has an uneven distribution of land and ocean, with most of the land in the northern hemisphere.

With definitions of diffusion and heat capacity, the timestep and latitude step which are numerically stable can be calculated. To do this the EBCM is investigated with a plane wave solution and boundaries on the timestep and latitude step are found. The explicit calculation of this is shown in appx. A, with the result that, for constant diffusion and timestep, a lower heat capacity requires a larger latitude step. The default values for the model are then taken as a timestep of $\Delta t = 1$ day and $S = 61$ latitude nodes ($\Delta \lambda = 3°$ separation). These parameters give good resolution while being completely numerically stable. For planets with $f_o = 0$ (see Sec. 3 C) a lower value of $S = 31$ is chosen as it is stable for the land-only heat capacity value.

WK97 provides three sets of IR-emission and Albedo functions. Following the example of SMS08 and Dressing10, the second set of IR and Albedo functions which are given by

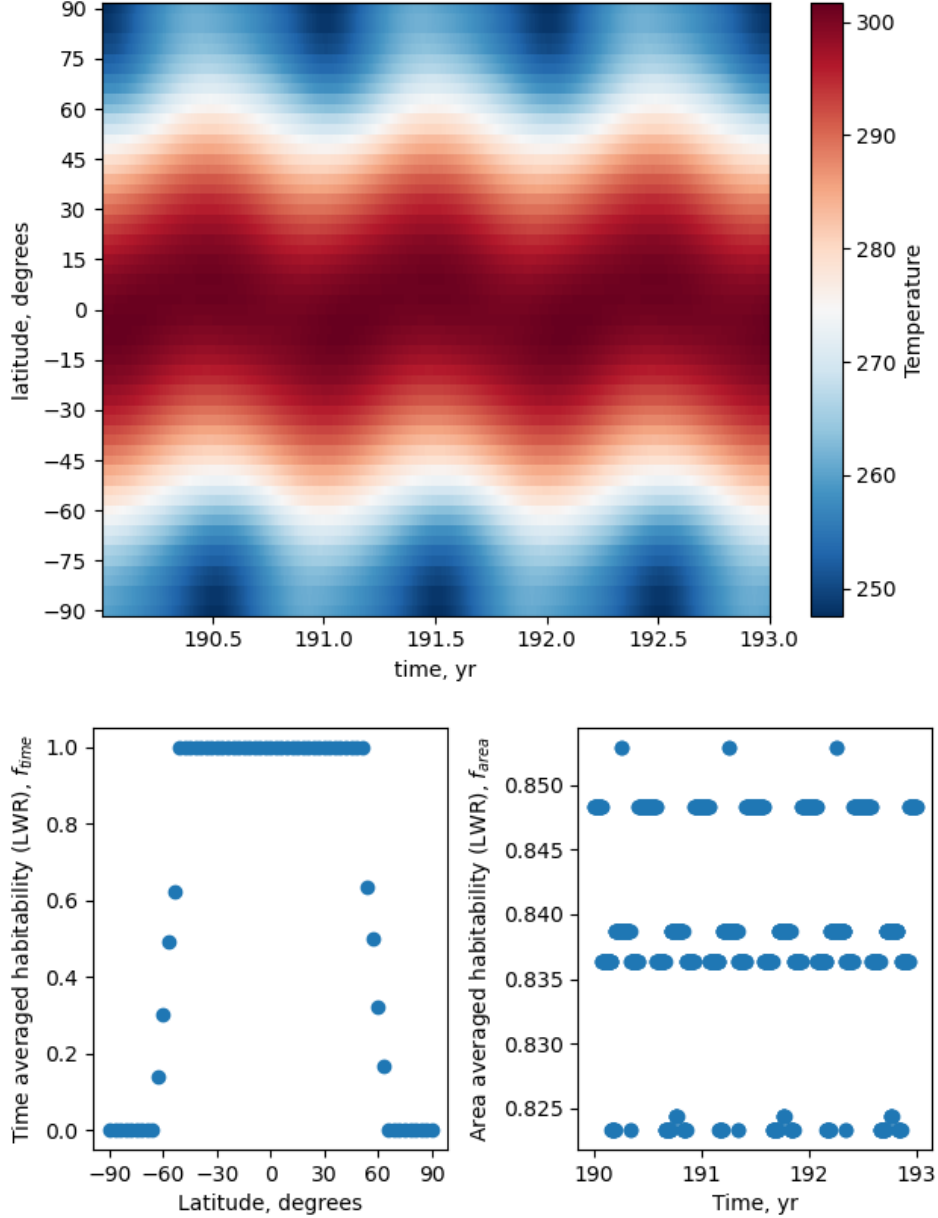$$I(T) = I_2(T) = \frac{\sigma T^4}{1 + 0.5925(T/273\text{K})^3} \tag{20}$$

FIG. 2: Top: The temperature distribution for the Earth model with parameters given in Table I. The time range is for 2 years, showing the periodicity of the seasons in the model. Bottom: The temperature distribution processed with the LWR habitability (eqn. (6)) and then averaged over time (left) or area (right).

$$A(T) = A_2(T) = 0.525 - 0.245 \tanh\left(\frac{T - 268\text{K}}{5}\right), \qquad (21)$$

are used in all models. This IR-emission is a blackbody radiation term (numerator) damped by the optical thickness of the atmosphere (denominator) which is roughly equivalent to the greenhouse gas effect due to water vapour content in the air. The albedo function is a smooth scaling from low reflectivity of land and forest to high reflectivity due to ice and snow.

The insolation function, S, is defined in WK97 as the day averaged incident (based on lati-

tude) radiation from the sun,

$$S(\lambda, t) = \frac{q_0}{\pi} \left(\frac{1 \text{ au}}{r(t)} \right)^2 (H(t) \sin \lambda \sin \delta(t) + \cos \lambda \cos \delta(t) \sin H(t)), \qquad (22)$$

where $q_0 = 1360$ Wm^{-2} is the insolation from the Sun, $r(t)$ is the distance from the Sun, $\cos H(t) = -\tan \lambda \tan \delta(t)$ is the radian half-day length with $0 < H < \pi$, and $\delta(t)$ is the solar declination defined by

$$\sin \delta(t) = -\sin \delta_0 \cos(L_s(t) + \pi/2), \qquad (23)$$

where δ_0 is the obliquity of the planet and $L_s(t) = \omega t$ is orbital longitude from an orbital angular velocity found by Kepler's laws. It is important to average over a day insolation as the model does not have a longitude dimension, so cannot account for uneven distribution of the insolation, for example in the case of a tidally locked planet.

The distance from the Sun is variable due to eccentricity. For a 2-body system this distance can be calculated through an iterative method as follows

$$r(t) = a(1 - e \cos E(t)), \qquad (24)$$

where a and e are semimajor axis and eccentricity respectively, and the eccentricity anomaly E is given by iteration

$$\begin{aligned} E_0 &= M \\ E_{i+1} &= E_i + \frac{M + e \sin E_i - E_i}{1 - e \cos E_i}, \end{aligned} \qquad (25)$$

where $M = 2\pi(t + t_0)/T$ for a temporal offset t_0 and period of the orbit T. The error in this function inceases with higher e but reduces with additional iterations. Three iterations with an eccentricity of 0.9 gives an error in E of 5% (compared to 100 iterations), which is a good compromise between computation time and accuracy, especially as $e = 0.9$ is the upper bound for eccentricities considered.

The temperature distribution for the Earth model is shown in Fig. 2 for 2 years after 190 years of evolution. There is clear periodicity in the model corresponding clearly with the seasonal variations experienced by the Earth.

Also shown is the LWR habitability of this temperature data which has been time averaged with eqn. (32) and area averaged with eqn. (33). The time and area averaged habitability is $H_{\text{Earth}} = 0.84$, meaning that the Earth is, when using LWR, 84% habitable. When using HC habitability this value is slightly reduced but the same to two significant figures.

The time averaged habitability shows how the the equator is habitable all year around. The poles are uninhabitable year round. Between $65°$ to $45°$ the habitability decreases linearly, representative of the variablity of the frost line.

The area averaged habitability changes in steps as each discrete latitude band becomes habitable or uninhabitable. It is periodic, but difficult to predict within each year.

B. Discretisation and Time evolution

Numerically integrating the EBCM requires the derivatives to be discretised. Spatially the planet can be split into S latitude bands, separated by

$$\Delta\lambda = \frac{\pi^{\text{rad}}}{S-1} = \frac{180°}{S-1}, \tag{26}$$

with spatial indexing of each band from $m = 0, 1, \ldots, S-1$. Similarly, a temporal indexing of $n = 0, 1, \ldots$ is used to discretise time in steps of Δt. Thus T_n^m is the temperature at the mth timestep for the nth latitude band.

The spatial derivatives can then be approximated by the central difference and second order central difference:

$$\frac{\partial T_n^m}{\partial\lambda} = \frac{T_n^{m+1} - T_n^{m-1}}{2\Delta\lambda}, \tag{27}$$

$$\frac{\partial^2 T_n^m}{\partial\lambda^2} = \frac{T_n^{m+2} - 2T_n^m + T_n^{m-2}}{(2\Delta\lambda)^2}, \tag{28}$$

and the temporal derivative can be approximated as a forward difference,

$$\frac{\partial T_n^m}{\partial t} = \frac{T_{n+1}^m - T_n^m}{\Delta t}, \tag{29}$$

with numerical stability analysed in appendix A. Evolving the EBCM is performed by solving eqn. (29) for T_{n+1}^m in terms of the parameter and temperature values at timestep n.

However, a problem arises at the edges of the model as $m = -2, -1, S, S+1$ are not defined. To fix this the derivatives at $m = 0$ ($m = S - 1$) are discretised as forward then backward (backward then forward) derivatives. By imposing that $\partial T_n^{m=0,S-1}/\partial\lambda = 0$, the second order derivatives then reduce to

$$\frac{\partial^2 T_n^{m=0}}{\partial\lambda^2} = \frac{1}{\Delta\lambda}\left(\frac{\partial T_n^{m=1}}{\partial\lambda} - \frac{\partial T_n^{m=0}}{\partial\lambda}\right) \quad = \frac{T_n^{m=1} - T_n^{m=0}}{(\Delta\lambda)^2} \tag{30}$$

$$\frac{\partial^2 T_n^{m=S-1}}{\partial\lambda^2} = \frac{1}{\Delta\lambda}\left(\frac{\partial T_n^{m=S-1}}{\partial\lambda} - \frac{\partial T_n^{m=S-2}}{\partial\lambda}\right) = \frac{T_n^{m=S-2} - T_n^{m=S-1}}{(\Delta\lambda)^2}. \tag{31}$$

Furthermore, the treatment imposed for the $m = 1$ and $m = S - 2$ second order derivatives is much the same, using central-backward and central-forward derivatives respectively.

C. Averaging and Habitability

Analysing the data produced requires the use of area-weighted averaging and time averaging from SMS08. The original equations are given as continuous integrals, but are discretised in a similar way to the derivatives in 2 B. Thus the time averaging, area-weighted averaging, and total averaging are given by

$$Q_{p\to q}^m = \frac{\sum_{n=p}^q Q_n^m \Delta t}{\sum_{n=p}^q \Delta t} = \frac{\sum_{n=p}^q Q_n^m}{t_q - t_p} \tag{32}$$

$$\bar{Q}_n = \sum_{m=0}^{S-1} Q_n^m F^m = \sum_{m=0}^{S-1} \frac{1}{2} Q_n^m \cos(\lambda_m) \Delta\lambda, \tag{33}$$

$$\bar{Q}_{p\to q} = \frac{\sum_{n=p}^{q} \sum_{m=0}^{S-1} Q_n^m \cos(\lambda_m) \Delta\lambda}{2(t_q - t_p)}, \tag{34}$$

respectively, with the time averaging happening between a time t_p and t_q. These averages can now be used to evaluate if a model has reached an equilibrium temperature and what the average habitability of a planet is.

A model is said to reach an equilibrium temperature when the average temperature between 2 averaging periods divided by the average temperature over both periods is less than some tolerance ϵ:

$$\frac{\bar{T}_{p\to q} - \bar{T}_{q\to r}}{\bar{T}_{p\to r}} < \epsilon. \tag{35}$$

Typically the averaging occurs over an orbital period (i.e. local year), so the equilibrium temperature is when there are no significant variations in temperature between two consecutive orbits. The value of ϵ chosen directly influences how long the model must be run to reach an equilibrium. In most cases a value of $\epsilon = 10^{-3}$ is used and results in equilbrium times of between 20 and 150 years depending on model parameters. It is worth noting for some plots that a value of $\langle T \rangle = -1$ means the model did not reach an equilbrium temperature within the evolution time and value of ϵ. This $\langle T \rangle = -1$

The classical habitability function is the Liquid Water Requirement (LWR) given by

$$H_{\text{LWR}}(T) = \begin{cases} 1 & 0°\text{C} \le T \le 100°\text{C} \\ 0 & \text{Otherwise} \end{cases}, \tag{36}$$

Thus a temperature is habitable if it is between the boiling and melting points of water.

An alternative is motivated by the limits of human endurance, thus is called Human Compatibility (HC). If a human's core temperature is raised above $35°$C then enzymes esssential for life denature and breakdown. This does not mean temperatures above this are lethal as humans can regulate temperature by sweating. The wet bulb temperature is defined by wrapping a thermometer bulb with a wet cloth. It is designed to take the humidity and ambient temperature into account, essentially mimicking the internal temperature of a human. Thus a wetbulb temperature of $35°$C is lethal if prolonged.

This climate model does not calculate humidity, thus a conservative temperature at which habitability reduces is taken to be $30°$C:

$$H_{\text{HC}}(T) = \begin{cases} 1 & 0°\text{C} \le T \le 30°\text{C} \\ 0 & \text{Otherwise} \end{cases}, \tag{37}$$

with the additional constraint that temperatures greater than $40°$C or less than $-10°$C in a latitude band sets the habitability of the band to 0 for all time.
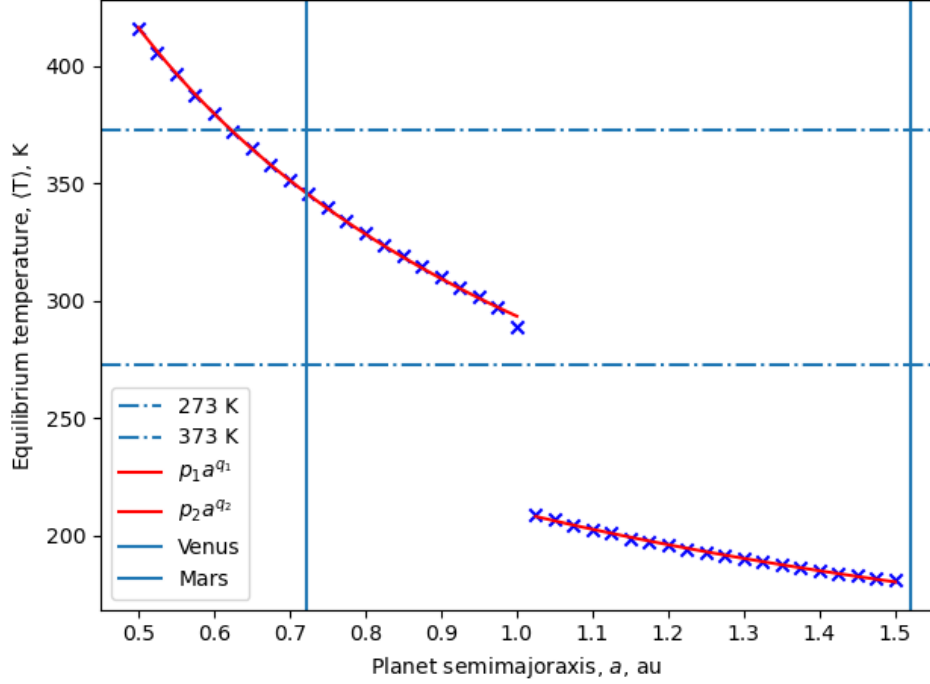
FIG. 3: A plot of the equilibrium temperature of the planet when varying its semimajor axis at constant eccentricity of $e = 0.0167$. Overlaid on the plot are two curves which are fitted to the data by a least squares regression. The form of the curve is $\langle T \rangle = p_i a^{q_i}$. Also shown are the orbits of Venus and Mars to highlight the range of values considered.

3. INVESTIGATING EARTH-LIKE EXOPLANETS

A. Varying semimajoraxis and eccentricity

General temperature relations for a planet can be found from the 0DEBM. Time averaged insolation of an planet in an elliptical orbit is given by

$$S = \langle F \rangle = \frac{q_0}{a^2\sqrt{1 - e^2}}, \tag{38}$$

where $q_0 = L_{\text{Sun}}/4\pi a_{\text{Earth}}^2 \approx 1360 \text{ Wm}^{-2}$ is the bolometric solar flux for Earth, a and e are the semimajor axis and eccentricity respectively of the planet [28].

By subsituting this relation into equation (1), the temperature of a planet can be related to semimajor axis and eccentricity through

$$T \propto a^{-\frac{1}{2}}(1 - e^2)^{-\frac{1}{8}}, \tag{39}$$

with proportionality constant $(q_0(1 - A)/4\sigma)^{1/4} = 255$ K for an Earth-like albedo of 0.3.

The validity of this proportionality can be investigated in terms of the semimajor axis by keeping $e = 0.0167$ constant and varying a from just outside Mercury's orbit at 0.5 au to Mars' orbit at 1.5 au. As seen in Figure 3 there are three main zones of interest to consider.

The first zone with $a < 0.65$ au has temperatures too high to sustain liquid water due to being too close to the Sun. The second zone with $0.65 < a < 1$ au is much more temperate,
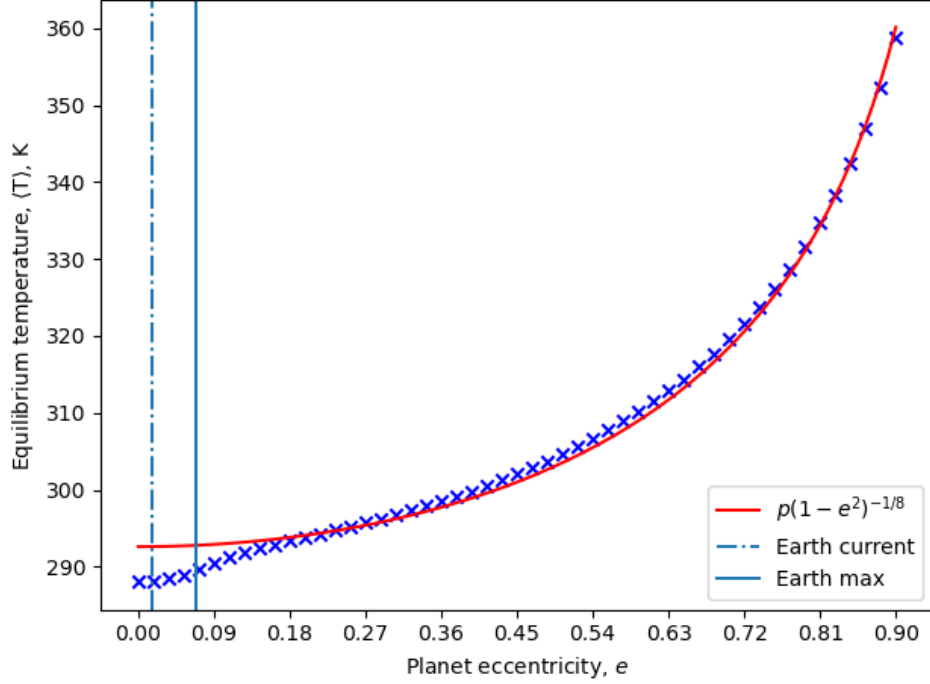
FIG. 4: A plot of the equilibrium temperature of the planet when varying its eccentricity at constant semimajor axis of $a = 1$ au. Overlaid on the plot is a curve which is fitted to the data by a least squares regression. The form of the curve is $\langle T \rangle = p(1 - e^2)^{-1/8}$. Also shown are the current and maximum theoretical value of Earth's eccentricity [27]. The minimum value is 0. There is a dip from the model at lower eccentricities due to IAB forming polar icecaps.

and is able to sustain liquid water on the planet's surface. Both the first and second zones are described by $\langle T \rangle = p_1 a^{q_1}$ with $p_1 = 293.5 \pm 0.4$ and $q_1 = -0.505 \pm 0.004$. q_1 is very close to the expected -0.5 powerlaw seen in eq. (39). However, the value of p_1 is ~ 38 K higher than the expected proportionality, most likely due to the additional greenhouse effect present in the 1D model.

The third zone with $a > 1$ au is a sudden departure from this expected powerlaw, with $p_2 = 210.2 \pm 0.2$ and $q_2 = -0.378 \pm 0.003$. This is due to IAB which works as follows. As the planet cools, ice forms with a higher albedo than the land or ocean. This higher albedo means more light is reflected, thus the planet absorbs less heat, so cools more. This cycle continues until the planet reaches a much colder equilibrium than is expected by a fixed albedo method. At 1 au the planet is on a tipping point in terms of this feedback loop, as seen by the temperature being slightly lower than expected by eqn. (39). This, along with the following analysis of eccentricity and obliquity, help show why the Earth has had many ice ages in the past [29].

Alternatively, a can be fixed at 1 au and the eccentricity can be varied from a perfect circle, $e = 0$, to a very eccentric ellipse, $e = 0.9$. Beyond $e > 0.9$ the iteration to find orbital distance converges much less quickly so becomes intractible. Additionally planets in extreme orbits with $e > 0.9$ would be extremely unstable and most likely would not be able to retain an atmosphere due to extreme temperatures.

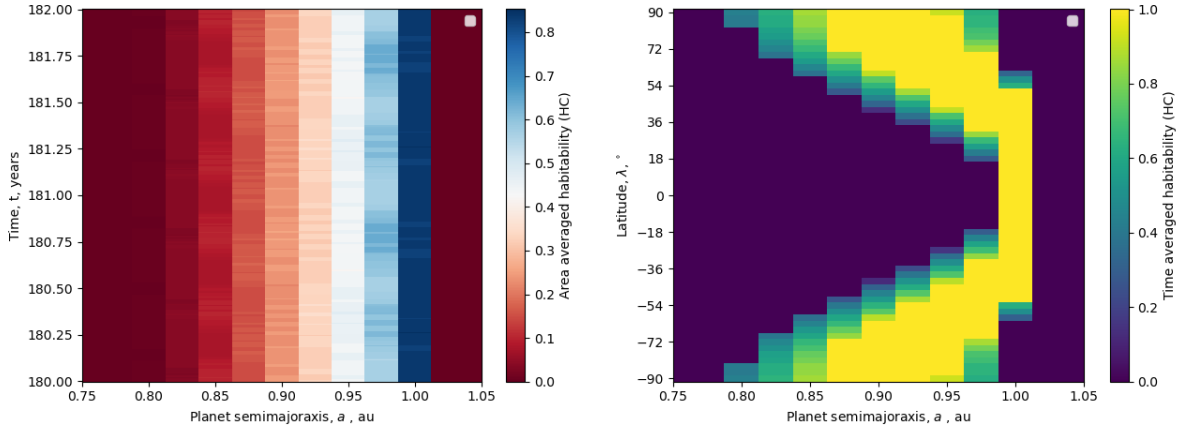Varying the eccentricity is similar to varying the semimajor axis. There are two main zones

15

FIG. 5: Left: A heatmap for area-averaged HC habitability for a 2 years on the y-axis and planet semimajor axis between 0.75 and 1.05 au on the x-axis. The planet is never 100% habitable, reaching a maximum of 85% when at the Earth-like 1 au. Right: A heatmap for the 10-year time-averaged HC habitability for each latitude band on the y axis and the same planet semimajor axis values on the x-axis. In this case some latitude bands do reach 100% habitability.

of interest in Figure 4 where the eccentricity of the planet is varied.

The zone with $e > 0.2$ follows the relationship well, and the globally averaged temperature doesn't exceed the boiling point of water. On the other hand, the zone with $e < 0.2$ is up to 5 K lower than the relationship. This dip is again due to IAB. High eccentricities mean the planet gathers and stores enough thermal energy when close to the Sun to prevent polar ice caps from forming even when further away from the Sun. Lower eccentricities allow for polar ice caps to form which then significantly lower the global temperature.

As seen from the vertical lines in Fig. 4, the Earth has moved in this lower eccentricity region for its entire history, suggesting that the presence of the polar caps has been reasonably constant for the recent past.

In Fig. 5 the semimajor axis of the planet is varied between just outside Mercury's orbit and Mars' orbit at constant eccentricity in order to investigate how HC habitability changes. The area-averaged habitability shows slight variations in habitability over time. This variation occurs for two main reasons: the growth and recession of the polar icecaps and equatorial desert. This growth and recession is shown in the time-averaged habitability where polar and equatorial regions have habitabilities between 0 and 1, indicating they are partially habitable over time.

As a decreases from 1 au, the planet experiences higher insolation. This higher insolation gives rise to higher temperatures across the planet. This melts the poles which are otherwise frozen, and causes the already hot equator to become too hot to sustain life.

Slighty increasing a from 1 au, the planet experiences a sharp drop in temperature. This is due to IAB where a small temperature decrease allows the icecaps to grow, and further decrease insolation until the entire planet is covered in ice.

In this case the HC habitability means that an Earth-like planet would not be habitable at the orbits of our closest neighbours, Venus and Mars.

Similarly, Fig. 6 shows the effects on habitability when the eccentricity of the planet is varied from 0 to 0.9. At low eccentricities, such as those the Earth has experienced in it's history, there
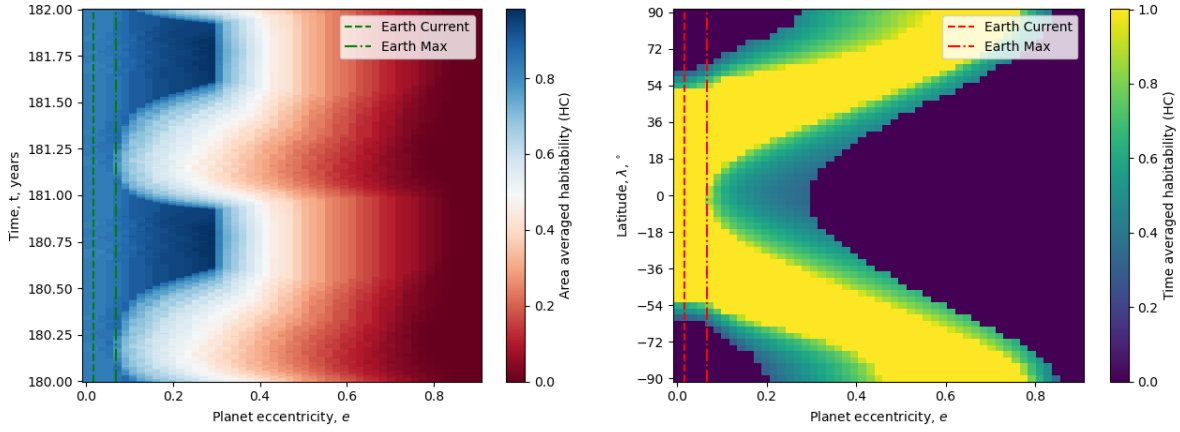
FIG. 6: Left: A heatmap for area-averaged HC habitability for a 2 years on the y-axis and planet eccentricity between 0 and 0.9 on the x-axis. The planet is never 100% habitable, reaching a maximum of 85%. Right: A heatmap for the 10-year time-averaged HC habitability for each latitude band on the y axis and the same planet eccentricity values on the x-axis. As eccentricity increases the habitable zones of the planet move outwards towards the poles because they are less directly insolated.

is little variation both in area- and time-averaged habitabilites.

Increasing eccentricity results in more seasonality. For example for $e = 0.2$ the planet has an area averaged habitability which starts at 0.5, increases to 0.85, then decreases again at the turn of the year. This is because the planet's temperature is too hot in the first half of the year near the Sun, and is temperate all over the planet for the other half of the year as the planet is allowed to cool away from the Sun. However for eccentricities $e > 0.3$ the hot spike as the planet is close to the Sun exceeds the maximum limit and latitude bands at the equator are considered fully uninhabitable. This results in a sizeable decrease in habitability for the other half of the year where the planet is cooling.

At extreme values of eccentricity, only the poles stay cool enough year round to harbour life. However, this represents a small fraction of the surface area of the planet. At eccentricites above $e > 0.8$ the poles become too hot for life at certain parts of the year, and eventually are totally uninhabitable.

So far the semimajor axis and eccentricity have been varied independently to investigate effects on the time and area habitabilites. Varying both together can illuminate the habitability parameter space for orbits in exoplanet systems. This is shown in Fig. 7 where the semimajor axis and eccentricity of a planet are varied together. The top graph is a heatmap for the equilibrium temperature of the planet, and the bottom graphs are the processing of the temperature data using the LWR habitability and HC habitability which are then time and area averaged.

The temperature heatmap highlights the drop off in temperature when IAB starts and the planet falls into a snowball. There exist some above freezing temperatures for high eccentricity and high semimajor axis, likely due to the planets unfreezing when close the Sun, and refreezing when further away.

Both habitabilites show similar shapes with different widths which is reflective of HC being more restrictive in temperature range than LWR. The differnce in the habitabilites is shown at high eccentricity. The LWR habitability suggests that there is a wide range of semimajor axis
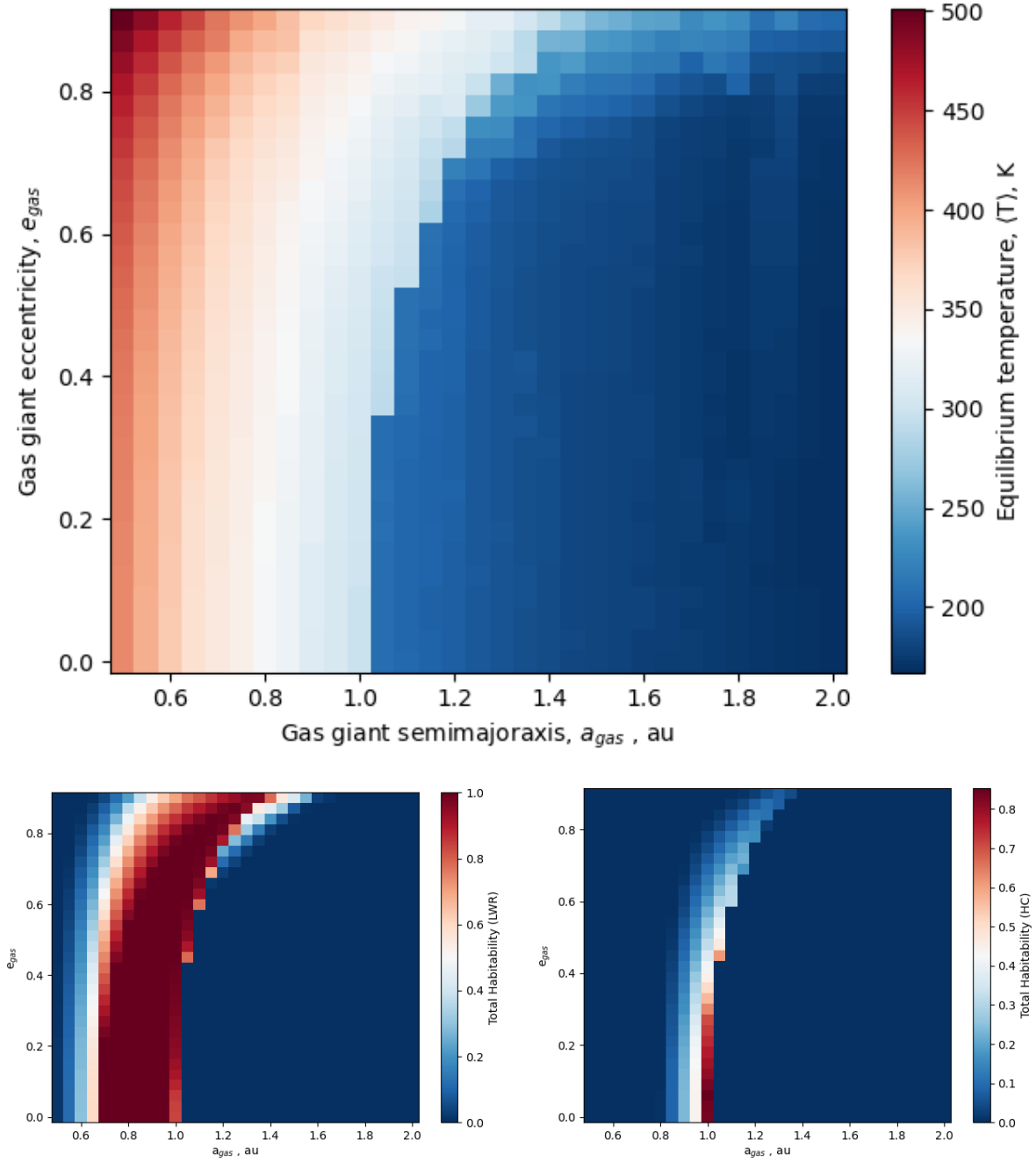
FIG. 7: Top: Varying the semimajoraxis and eccentricity of the gas giant to produce a heat map for the equilibrium temperature of the planet. Left: Processing of the temperature data with eqn. (6). Right: Processing of the temperature data with eqn. (7).

values where liquid water exists on the surface of the planet year-round at high eccentricities. Alternatively, the HC habitability indicates that high eccentricities have extremes of temperature which are not compatible with life, thus the actual habitability is lower.
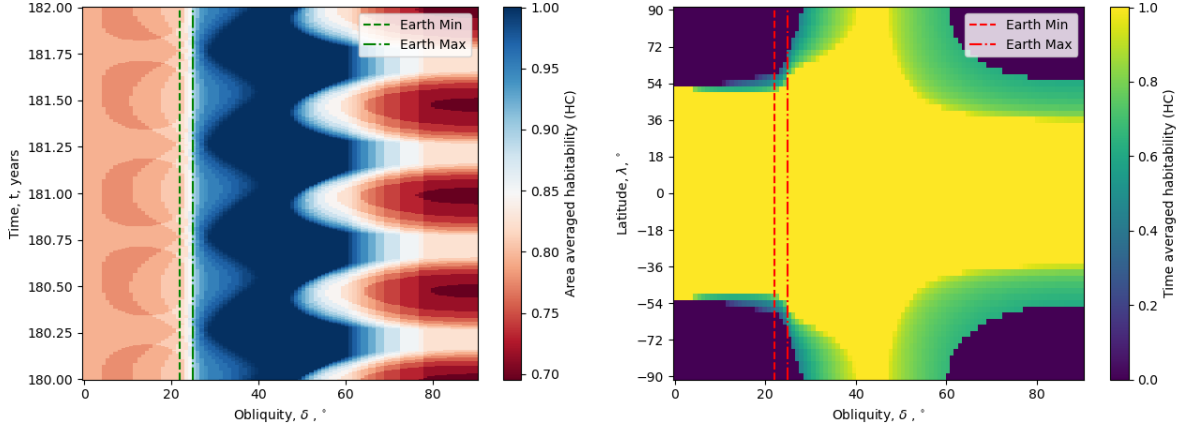
FIG. 8: Left: The area-averaged human habitability for a 2 year period after 150 years of simulation. The habitability varies between 70% and 100%, with the highest habitabilities being between 20°and 50°At lower obliquities polar ice caps form reducing the area habitability. Right: The 10 year time-averaged human habitability for each latitude band. Habitability at the equator of this planet is usually totally habitable all year around.

B. Varying obliquity

The obliquity of the planet's spin can be varied to see how the habitability profile changes. Due to the uniform nature of the planet there is a symmetry about $\delta = 90°$. Because of this symmetry only values between $0°$ and $90°$ need to be considered.

Varying obliquity is shown in Fig. 8. There are three main areas to consider:

- Low obliquity ($0° - 20°$) where the planet directly presents its equator to the Sun for the majority of it's orbit.

- Medium obliquity ($20° - 50°$) where the planet presents both the equator and poles to the Sun in roughly equal amounts.

- High obliquity ($50° - 90°$) where the planet cycles between presenting a pole to the Sun and presenting the equator (sideways) to the Sun.

For low obliquities there are small habitability variations. These variations are due to the permanent icecaps growing and shrinking. As the cap grows more latitude bands are below freezing so area-averaged habitability decreases. As the cap shrinks the opposite occurs, and area-averaged habitability increases. At especially low obliquities the shrinking and growing is smaller than the width of a latitude band so the habitability is constant.

At medium obliquities the icecaps are insolated directly enough to be melted. At the lower end of this range the icecaps can reform for the portion of the year that they are facing away from the Sun, and then melt in the portion of the year when facing toward the Sun. This results in some seasonal habitability. In the middle of this range the poles are melted for the entire year. This suggests an optimal range for obliquity where the insolation is spread out evenly across the planet, allowing for the entire surface to be temperate (and thus habitable) for all time.
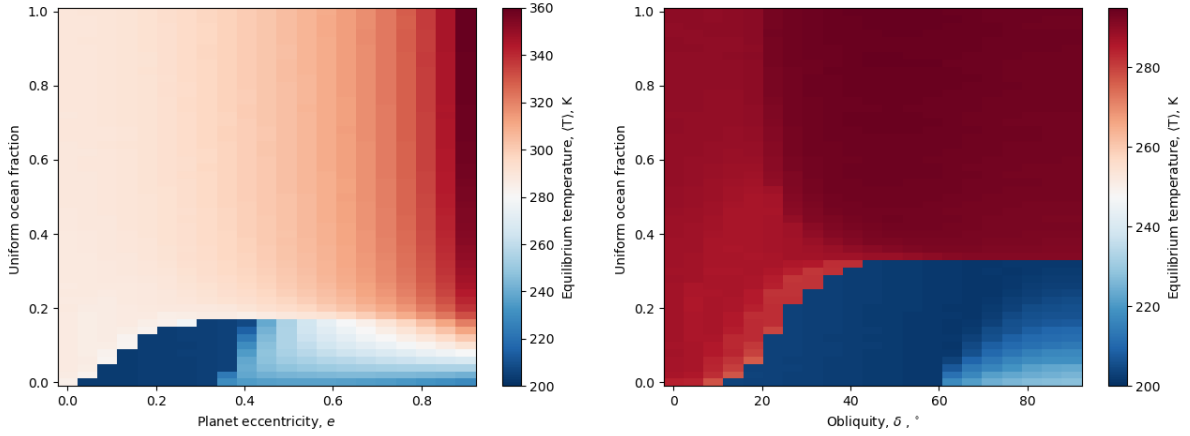
19

FIG. 9: A heatmap for equilibrium temperature when varying ocean fraction with eccentricity (Left) and obliquity (Right). The two main regions in both graphs are the warm temperatures with higher ocean fraction and much colder temperatures with lower ocean fractions. While both temperature scales start at 200 K, the eccentricity graph reaches 360 K whereas the obliquity graph reaches 295 K.

At very high obliquities each pole is either directly insolated or in shadow for long periods of time, so experience extreme temperatures. The pole which is being directly insolated becomes very hot and can exceed the maximum temperature which sets the habitability of the latitude band to 0 for all time. Conversely, the pole which is in constant shadow quickly cools and freezes over. This exceeds the minimum temperature for habitability. Between the poles is a steep temperature gradient from hot to cold pole. This gives rise to the 80% habitability regions between dark spots where the habitability is at its highest for large obliquity.

As the planet moves in the orbit the equator is directly insolated and both poles are only partially insolated. The equator has a much larger area so can distribute this extra heat better so exceeds the habitable limit but not the maximum temperature. The poles at this time are able to melt or cool as appropriate. While the temperatures they reach at this time may be suitable for life, they exceeded the maximum limit so are still considered uninhabitable. The overall effect are seen in the darker 70% habitable regions where the poles and equator both have reduced habitability.

Most planets have obliquities which can vary through this entire range of values. The Earth is an exception to this. The Moon stabilises the Earth's obliquity to vary between $22°$ and $25°$ with a current value of $23.5°$ (decreasing). In this range the habitability is fairly constant.

C.   Varying ocean fraction with eccentricity and obliquity

The snowball state produced by IAB has been seen when varying semimajor axis (Figs. 3 and 5) and partially when varying eccentricity (Fig. 4). A variable which influences susceptibility to IAB is the ocean fraction.

The thermal timescale (eqn. (3)) means that ocean, which has a higher heat capacity than land, has a larger thermal inertia. Larger thermal inertia means the ocean on the planet helps to reduce temperature variations which the planet experiences. Thus it is expected that planets with low ocean fraction will be susceptible to IAB in shorter timescales or with less forcing

than high ocean fraction planets. The main orbital variables influencing this forcing are the eccentricity and obliquity.

In an eccentric orbit the insolation decreases as the planet moves away from the Sun. This reduced insolation causes a lower temperature for a portion of the year. If the temperature is reduced enough, IAB can kick in and cause the planet to fall into a snowball state that it cannot recover from.

Obliquity can also cause snowball states. Obliquity for the Earth means seasons, where winter occurs in a hemisphere when that hemisphere points away the Sun because it is less directly insolated. The severity of this winter depends on how much of the pole is in permanent shadow and how long the winter lasts. Permanent shadow is influenced by the obliquity of the planet, and the length of the winter depends on the period of the orbit. Varying obliquity will allow for the investigation of the permanent shadow effect.

To investigate these expectations the ocean fraction of the model is varied in Fig. 9. In the left plot ocean fraction is varied against eccentricity with zero obliquity, and in the right plot ocean fraction is varied against obliquity with zero eccentricity.

We see that for eccentricity there as a minimum ocean fraction which increases with eccentricity until a maximum at $e = 0.3$ of $f_{\text{ocean}} = 20\%$. At $e = 0$ there is no temperature variation, so the model cannot fall into a snowball state. As eccentricity increases the minimum ocean fraction, thus minimum thermal inertia, required to prevent a fall into a snowball state increases as expected. Unexpected is the region after $e > 0.4$.

At much higher eccentricities and low ocean fraction the planet moves further from the Sun so falls into a snowball state more easily. It can also move closer to the Sun which then increases the insolation. This insolation can be higher enough to allow the planet to melt and leave the snowball state. The combination of these two effects is that the planet is very hot half of the year and frozen for the other half of the year, with an average temperature which is habitable.

The habitability of this sort of planet is difficult to quantify. Humans have survived iceages in the past by burning fuels and sheltering in caves, to give just two examples. We are yet to see if human life will survive extreme heat.

In a similar way when varying obliquity the minimum ocean fraction starts at 0 and increases until a maximum at roughly $\delta = 45°$. For $0° < \delta < 10°$ the planet does not fall into a snowball state as the permanent shadow region is not large enough to cause runaway IAB.

For Earth-like obliquities (between $22°$ and $25°$) the planet is susceptible to a snowball state only if the planet has ocean fraction less than roughly 15%.

At very high obliquities (and low ocean fractions) the pole which faces the Sun can be melted. This is because low ocean fraction has low heat capacity, so the heat input from the direct insolation to the polar region can raise the temperature of the region very easily. This is very localised to the polar region and so only slightly raises the average temperature of the planet.

The minimum ocean fraction for the obliquity case is much larger than the eccentricity case. This is indicative that the temperature variations due to obliquity are much larger than variations due to eccentricity. This is likely due to the obliquity having a more localised effect on the polar regions of the planet as opposed to eccentricity's planetwide effect.

Both variables cause the planet to be susceptible to IAB, and both cause full or partial recovery from snowball at extreme values. For eccentricity the minimum ocean fraction varies ap-
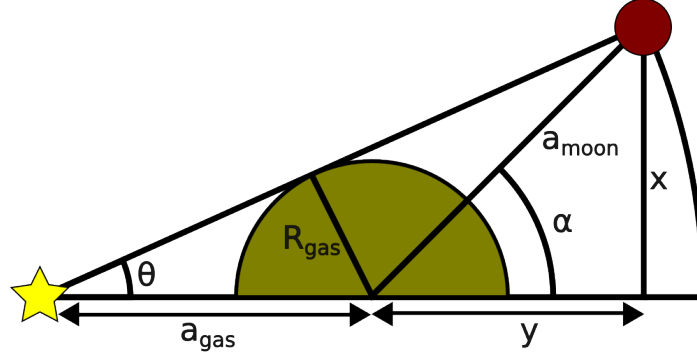
FIG. 10: A diagram of a gas giant (middle green hemisphere) in orbit around a star (left yellow shape) at a distance a_{gas}, and a moon (top right maroon circle) in orbit of the planet at a distance a_{moon}. The planet has radius R_{gas}. The angle θ corresponds to half the angular size of the planet from the star. Inside the angle 2α the moon is eclipsed by the planet. The eclipsing fraction is thus defined as fraction of the orbit which is in shadow, $\epsilon = 2\alpha/2\pi$.

proximately quadratically with eccentricity until $e = 0.4$ where the eccentricity is high enough to melt the induced snowball meaning the time averaged temperature increases. The minimum ocean fraction in the obliquity case varies with an 'S' shape and levels out after $\delta = 40°$ to a minimum ocean fraction of $f_{ocean, min} = 0.36$. Similar to the eccentricity case, high obliquities can partially recover from the snowball. In this case it is due to the pole facing the Sun melting for half a year due to constant insolation before refreezing when facing away from the Sun. There are nearly no variations due to changing ocean fraction above $f_{ocean} = 0.2$ in the eccentricity case, and few variations above $f_{ocean} = 0.4$ for the obliquity case.

4. EARTH-LIKE EXOMOON MODIFICATIONS AND RESULTS

A. Eclipsing

In order to add eclipsing to the model it must be known when the moon is behind the gas giant such that the sun is blocked. When modelling eclipsing, the gas giant and moon are assumed to have co-planar orbits such that the full radius of the gas giant is used. It is also assumed that in the umbra the moon is fully eclipsed, and in the penumbra the moon is half eclipsed. In reality the penumbra varies between 0% eclipsed at the outer edge to 100% eclipsed at the edge to the umbra.

Initially, the eclipsing was quantified by solving for the distances and angles of the gas giant and moon using eqns. (24) and (25). The eccentric anomaly, E, is related to the true anomaly, ν, by,

$$\cos \nu = \frac{\cos E - e}{1 - e \cos E},$$ (40)

where e is the eccentricity of the orbit. By finding the x-y coordinates of the gas giant and moon, when the moon is eclipsed can be found. Due to the length of the eclipses a timestep of an hour must be used to evolve this eclipsing model. This would be impractical to run along side the 1 day timestep of the EBCM especially as the iteration process for finding the eccentric anomaly
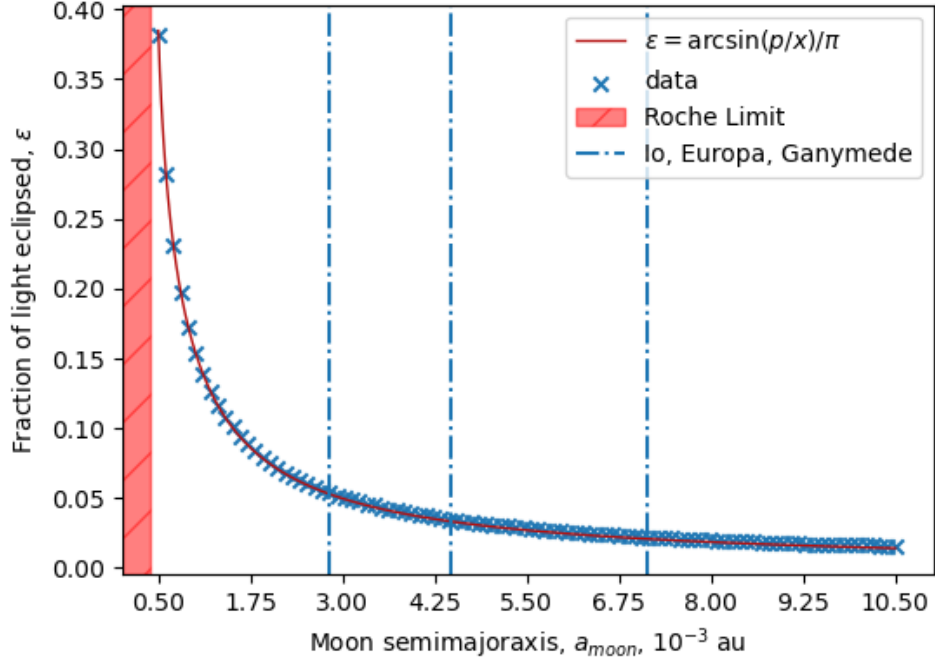
FIG. 11: Fraction of light eclipsed by a Jupiter sized gas giant when varying a moon's semimajor axis. Shown is the Roche limit for Jupiter, as well as the orbital distances of Jupiter's three innermost moons. Overlaid on the data is a fit of $\epsilon = \arcsin(p/x)/\pi$ with parameter $p = (4.675 \pm 0.005) \times 10^{-4}$ au.

is time consuming. Varying the 4 orbital parameters in the eclipsing model gives insight into the eclipsing however. Varying the eccentricity of the gas giant between 0 and 0.9 has a random effect on the eclipsing between the values 5% and 5.2%, and increasing eccentricity of the moon from $e = 0$ to 0.1 decreases the eclipsing from 5.07% to 5.02%. Varying the gas giant semimajor axis between 0.5 au and 10 au caused variation in the eclipsing fraction between 5% and 6%. The most important influence to the eclipsing was moon semimajor axis. Varying between 0.5 mau and 10.5 mau caused a decrease in eclipsing from 40% to 2% as seen in Fig. 11.

Knowing that the eccentricity of the orbits makes a negligible contribution to the motivates an analytical model with circular orbits. Using the assumption that the sun is a point source (valid if $a_{\text{gas}} \gg 10 a_{\text{moon}}$, which is true in the cases considered in this paper) the diagram shown in Fig. 10 is drawn and used to quantify the eclipsing fraction as follows.

In order to find the eclipsing angle, α, the distances x and y need to be found. The x distance relates the angular size of the gas giant from the sun, θ, to the eclipsing angle as

$$x = a_{\text{moon}} \sin \alpha = (a_{\text{gas}} + y) \tan \theta, \tag{41}$$

where the distance $y = a_{\text{moon}} \cos \alpha$ using the smaller triangle. Using the larger triangle, the angular size of the gas giant can also be found to be

$$\sin \theta = \frac{R_{\text{gas}}}{a_{\text{gas}}}, \tag{42}$$

which can then, in the small angle approximation that $\sin \theta = \tan \theta$, be related to the $\tan \theta$ term in eqn. (41). This leads to the relation of eclipsing angle to the radius of gas giant, and

23

semimajor axes of the moon and gas giant as follows,

$$\frac{R_{\text{gas}}}{a_{\text{moon}}} + \frac{R_{\text{gas}}}{a_{\text{gas}}} \cos \alpha = \sin \alpha. \tag{43}$$

This equation can be solved for the eclipsing angle in the sine term by using that $R_{\text{gas}} \ll a_{\text{gas}}$ so ignoring the cosine term. The eclipsing fraction, ϵ, can then be found by dividing 2 times the eclipsing angle by the full orbital angle 2π

$$\epsilon = \frac{2\alpha}{2\pi} = \frac{1}{\pi} \arcsin \frac{R_{\text{gas}}}{a_{\text{moon}}}. \tag{44}$$

This relation is investigated in Fig. 11 with a free parameter in place of R_{gas}. The value of the free parameter is $(7.013 \pm 0.008) \times 10^7$m which is extremely close to the radius of Jupiter, as to be expected.

B.   Reflectance and Emission from the Gas giant

Two sources of heat are indirectly from the star via the gas giant. First, light from the star can be reflected by the gas giant. The light absorbed by the gas giant is given by $S(1 - A_{\text{gas}})$, thus light reflected is given by SA_{gas}. This must be reduced by the distance, a_{moon}, and the eccentricity, e_{moon}, of the moon's orbit,

$$F_{\text{ref}} = \frac{SA_{\text{gas}}}{4\pi a_{\text{moon}}^2 \sqrt{1 - e_{\text{moon}}^2}}, \tag{45}$$

where $S = 1360 \text{ Wm}^{-2}$ is the same insolation as for the moon. The $4\pi a^2 \sqrt{1 - e^2}$ term in the denominator comes from eqn. (38) for average flux from a body. Second, IR emission from the gas giant can heat up the moon. This IR emission can have two sources, the first and most obvious is the gas giant being heated by the star and then reradiating that heat in equilibrium. This can be described using the 0DEBM (eqn. (1)) as

$$F_{\text{emit}} = \frac{4\pi R_{\text{gas}}^2 \sigma T_{\text{gas}}^4}{4\pi a_{\text{moon}}^2 \sqrt{1 - e_{\text{moon}}^2}} = \frac{R_{\text{gas}}^2 S(1 - A_{\text{gas}})}{4 a_{\text{moon}}^2 \sqrt{1 - e_{\text{moon}}^2}}, \tag{46}$$

where this flux assumes that the gas giant is in equilibrium as expected by the 0DEBM with the variables given in Table. II.. An alternative source is residual heat of formation. For example, Jupiter is still slightly warmer than expected from equilbrium [21]. This is not accounted for in this model, but could be added by setting the temperature directly instead of using the 0DEBM.

C.   Tidal heating

In the fixed-Q model, $-\text{Im}(k_2) = k_2/Q$, where k_2 is the second Love number for the moon and Q is the total dissipation factor due to friction, with both numbers constant. This model has some failings. The second Love number depends on material properties of the moon so will be directly influenced by the temperature of the mantle and core. These temperatures are also directly influenced by the amount of flux the moon receives due to tidal and radiogenic

Moon				Gas Giant		
Semimajor axis	Eccentricity	Radius	Density	Mass	Radius	Albedo
0.03 au	0.006	6.4×10^6 m	5500 kg m^{-3}	1.9×10^{27} kg	7.0×10^7 m	0.3

TABLE II: A summary of the default parameters for the Earth-like exomoon model. The moon orbital parameters are ones which generate a good level of tidal heating, and the radius and density are similar to the radius and density of the Earth. The gas giant parameters are the same as Jupiter's [30], where the volumetric mean radius, and bond albedo have been used. Other model parameters are the same as the planetary model (Tab. I).

heating. This model is not responsive to this dynamic temperature dependence and requires a single temperature of the core to be picked.

Alternatively, viscoelastic models allow for the core temperature to vary with respect to the amount of flux from tidal heating. To do this the stable point where tidal flux is equal to convective cooling for the core is found. Both the tidal heat and convective cooling are dependent on temperature of the core, thus this method finds temperature of the core at equilibrium. The implicit assumption here is that the moon has been in orbit long enough to have reached equilibrium between the tidal heating and convective cooling. This paper uses the Maxwell model from Henning et al [26], given by

$$-\mathrm{Im}(k_2) = \frac{57\eta\omega}{4\beta \left[1 + \left(1 + \frac{19\mu}{2\beta}\right)^2 \left(\frac{\eta\omega}{\mu}\right)^2\right]} \tag{47}$$

where $\beta = \rho g R_{\mathrm{moon}}$ has been described as gravitational stiffness term with ρ being the density of material in the moon, g being the moon's surface gravity, and R being the radius of the moon. The temperature dependent forms of the viscosity, η, and shear modulus, μ, are given in Henning et al [24] and in appx. B. The orbital frequency, ω, and other parameters take (or can be derived from) the default values in Tab. II.

The tidal heating can sharply cut off for certain orbital parameters when the tidal heating is less than convective cooling at all mantle temperatures so the core temperature at equilbrium is too low to heat the surface of the planet effectively.

D.   Impact on previous results

With the model appropriately updated, temperature profiles and habitabilities seen previously can be investigated for this moon model. Shown in Fig. 12 is how the time-averaged (HC) habitability for variable semimajor axis changes between the planetary model and moon model (left) and how the equilibrium temperature changes with semimajor axis (right). The plot on the left shows how the latitude habitable zone changes between a planetary model and a moon model with the default parameters in Tab. II. And the plot on the right shows how the equilibrium temperature of the planet between the planetary model and two moon models, one with default parameters and one with higher eccentricity.

The habitable zone becomes wider at all latitudes and moves outwards towards Mars' orbit. The reason for both these effects is the additional energy flux from tidal heating. The hab-
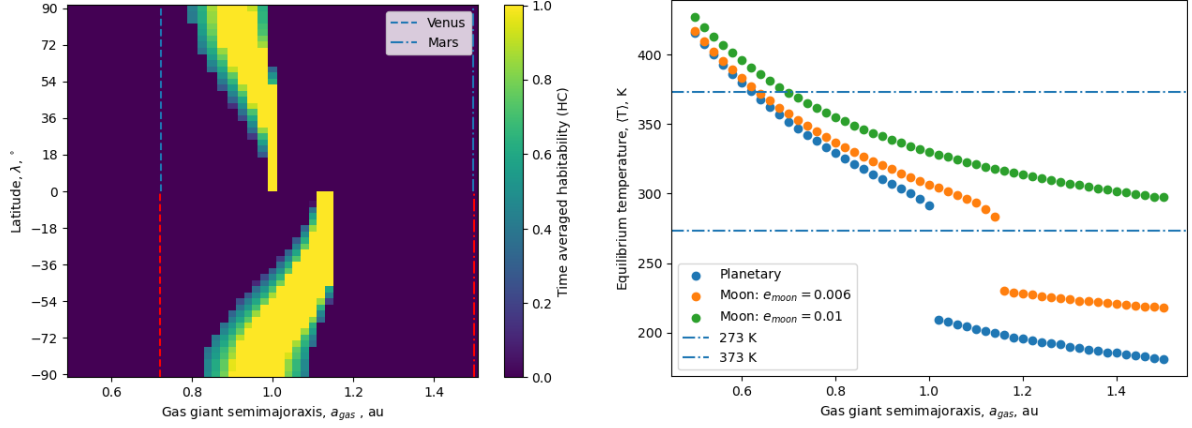
FIG. 12: Left: Comparison of the time-averaged (HC) habitability for variable semimajor axis for the planetary model (top) and moon model (bottom). The moon model has the default parameters in Tab. II. Right: Comparison of the equilibrium temperatures when varying gas giant semimajor axis for the planetary model (blue), and two moon models with different eccentricity (orange and green). Also shown are horizontal lines for the freezing and melting points of water.

itable zone becomes wider as the moon is less reliant on a specific distance from the Sun to generate habitable temperatures. The habitable zone moves further out as the additional energy flux generally raises the temperature of the planet, meaning it is too hot for life at the closer distances.

This is also seen in the equilibrium temperatures, where a wider range of values are within the range for liquid water. Seen in the orange set of data is a more exaggerated curve when falling to the snowball state than for the planetary model in blue. This is due to IAB playing less of a role in determining the climate of the planet as the tidal heating is independent of albedo. The tidal heating also helps to prevent the planet's temperature from decreasing to the point where IAB can dominate by providing a constant heat source when further from the star.

eccentricity: The temperature generally increases. The dip at low eccentricity due to IAB is missing from the moon models. This is due to the generally higher temperature

obliquity: Temperature increases. Temperature range decreases due to insolation playing smaller role (proportionally) in determining the planet climate. The variations due to obliquity become smaller as any insolation variation across the planet are dampened by the uniform tidal heating.

E.   Exomoon specific results

14 Variable moon semimajoraxis has a similar shape to the variable gas semimajoraxis.

At high semimajor axis the tidal heating is less than the convective cooling, so 'turns off'. It might be expected that the moon at the same distance as the Earth from the Sun would still be warm enough to be habitable. The high semimajoraxes and low eccentricities show that this is not the case as they are in snowball states. This is because to the reduction of insolation due to eclipsing is larger than the additional light reflected and emitted from the gas giant. As shown in Fig. 3 even a small decrease in insolation, such as the decrease due to eclipsing, can lead to
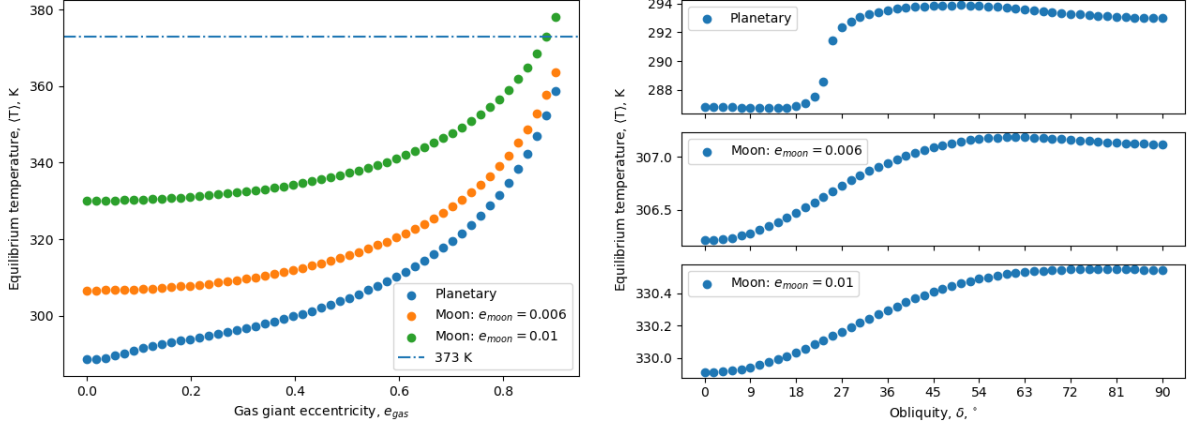
FIG. 13: Left: Comparison of the equilibrium temperatures when varying eccentricity for the planetary model (blue), and when varying gas giant eccentricity two moon models with different moon eccentricities (orange and green). Right: Comparison of the equilibrium temperatures when varying obliquity for the planetary model (top) and two moon models with different eccentricity (middle and bottom). The y-axes are very different, as each has progressively smaller range in values.
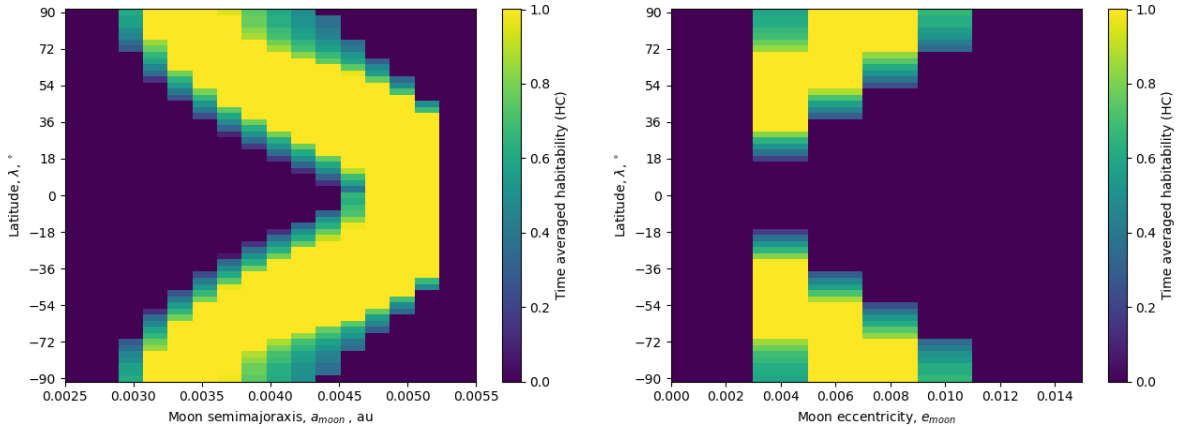

FIG. 14: Left: Time-averaged temperature heat map for each latitude band when varying moon semimajoraxis. Right: Time-averaged temperature heat map for each latitude band when varying moon eccentricity.

a snowball state.

5. DISCUSSION

Research motivated by climate change suggests that ice melting can release CO_2 which is not accounted for in this model. This would introduce a ice-temperature feedback where melting ice releases CO_2, increasing greenhouse gas effects and feeding back until the temperature is very high. This would reduce the habitability at higher temperatures particularly where the icecaps melt due to a higher CO_2 fraction in the atmosphere, thus larger greenhouse effect. However this effect is very particular for the Earth due to it's CO_2 rich past. It would not be correct to

assume that all exoplanets have a CO_2 rich past but could be considered in further research.

Ice melting and rising temperatures would also cause the oceans to expand, thus changing the mixing depth (thus heat capacity) of the oceans.

The approximation of a uniform planet could also be probed further. Exoplanets may have land-ocean distributions similar to Earth where the northern hemisphere has more land than the southern hemisphere. The planet could be probed with different fractions of land and ocean. For example: an ocean centered on one of the poles of the planet and increasing in size from a desert world with small a polar ocean to ocean world with a small polar continent.

6. CONCLUSION

REFERENCES

[1] ESA, "A brief introduction to exoplanets." `https://sci.esa.int/web/exoplanets/-/60654-a-brief-introduction-to-exoplanets`. Accessed: 2024/03/05, Last updated 2019/09/01.

[2] D. N. et al, "KOI-142, The king of transit variations, is a pair of planets near the 2:1 resonance," ApJ, vol. 777, no. 1, 2013.

[3] K. Lewis and et al, "Possibility of detecting moons of pulsar planets through time-of-arrival analysis," ApJ, vol. 685, no. 2, 2008.

[4] D. Kipping, S. Fossey, and G. Campanella, "On the detectability of habitable exomoons with kepler-class photometry," RAS, vol. 400, no. 1, 2009.

[5] M. Limbach and E. Turner, "On the direct imaging of tidally heated exomoons," ApJ, vol. 769, no. 2, 2013.

[6] M. Limbach and et al, "On the detection of exomoons transiting isolated planetary-mass objects," ApJ, vol. 918, no. 2, 2021.

[7] Exoplanet Team. `https://exoplanet.eu`. Accessed: 2024/03/05, Last update: 2024/03/04.

[8] NASA, "Artemis plan." `https://www.nasa.gov/specials/artemis/`. Accessed: 2024/03/06.

[9] CNSA, "China and russia sign a memorandum of understanding regarding cooperation for the construction of the international lunar research station." `https://www.cnsa.gov.cn/english/n6465652/n6465653/c6811380/content.html`. Accessed: 2024/03/06.

[10] M. Gillon, A. Triaud, B. Demory, and etal, "Seven temperate terrestrial planets around the nearby ultracool dwarf star TRAPPIST-1," Nature, vol. 542, 2017.

[11] O. C. et al, "Heating of the atmospheres of short-orbit exoplanets by their rapid orbital motion through an extreme space environment," ApJ, vol. 962, no. 2, 2024.

[12] G. V. L. etal, "Airy worlds or barren rocks? on the survivability of secondary atmospheres around the TRAPPIST-1 planets," A&A, 2024. Awaiting Publication, `https://doi.org/10.48550/arXiv.2401.16490`.

[13] North and Coakley, "Differences between seasonal and mean annual energy balance model calculations of climate and climate sensitivity," J. Atmos. Sci., vol. 36, no. 7, 1979.

[14] Williams and Kasting, "Habitable planets with high obliquities," Icarus, vol. 129, no. 1, 1997.

[15] D. Spiegel and et al, "Habitable climates," ApJ, vol. 681, no. 2, 2008.

[16] D. Spiegel and et al, "Habitable climates: the influence of obliquity," ApJ, vol. 691, no. 1, 2009.

[17] C. Dressing and et al, "Habitable climates: the influence of eccentricity," ApJ, vol. 721, no. 2, 2010.

[18] Y.-C. Lu and D. Romps, "Is a wet-bulb temperature of 35c the correct threshold for human survivability?," Environ. Res. Lett., vol. 18, no. 9, 2023.

[19] D. Williams, J. Kasting, and R. Wade, "Habitable moons around extrasolar giant planets," Nature, vol. 385, 1997.

[20] D. Williams, "Capture of terrestrial-sized moons by gas giant planets," Astrobiology, vol. 13, no. 4, 2013.

[21] L. Li, X. Jiang, R. West, and et al, "Less absorbed solar energy and more internal heat for jupiter," Nat Commun, vol. 3709, no. 9, 2018.

[22] C. Yoder and S. Peale, "The tides of io," Icarus, vol. 47, no. 1, 1981.

[23] Segatz and et al, "Tidal dissipation, surface heat flow, and figure of viscoelastic models of io," Icarus, vol. 75, no. 2, 1988.

[24] V. Dobos and E. Turner, "Viscoelastic models of tidally heated exomoons," ApJ, vol. 804, no. 1, 2015.

[25] V. Dobos, R. Heller, and E. Turner, "The effect of multiple heat sources on exomoon habitable zones," A&A, vol. 601, no. 91, 2017.

[26] W. G. Henning and et al, "Tidally heated terrestrial exoplanets: viscoelastic response models," ApJ, vol. 707, no. 2, 2009.

[27] J. Laskar, A. Fienga, M. Gastineau, and H. Manche, "La2010: a new orbital solution for the long-term motion of the earth," A&A, vol. 532, 2011.

[28] A. Méndez and E. Rivera-Valentín, "The equilibrium temperature of planets in elliptical orbits," ApJL, vol. 837, no. 1, 2017.

[29] C. Emiliani, "The cause of the ice ages," Earth and Planetary Science Letters, vol. 37, 1978.

[30] NASA, "Jupiter fact sheet." https://nssdc.gsfc.nasa.gov/planetary/factsheet/jupiterfact.html. Accessed: 2024/03/01.

Appendix A: Numerical stability of the 1D EBCM

Appendix B: Tidal heating equations and method

$$
\eta = \begin{cases}
\eta_0 \exp\left(E_a/RT\right) & T < T_s \\
\eta_0 \exp\left(E_a/RT\right)\exp\left(-B\phi\right) & T_s < T < T_b \\
10^{-7} \exp\left(40000\text{K}/T\right)(1.35\phi - 0.35)^{-5/2} & T_b < T < T_l \\
10^{-7} \exp\left(40000\text{K}/T\right) & T_l < T
\end{cases}
\tag{B1}
$$

$\eta_0 = 1.6 \times 10^5$ Pa s $T_s = 1600$ K $T_l = 2000$ K $T_b = T_s + f(T_l - T_s) = 1800$ K for $f = 0.5$
$E_a = 3 \times 10^5$ J.mol^{-1}

$$
\mu = \begin{cases}
5 \times 10^{10} & T < T_s \\
10^{\frac{8.2 \times 10^4 \text{K}}{T} - 40.6} & T_s < T < T_b \\
10^{-7} & T_b < T
\end{cases}
\tag{B2}
$$

SCIENTIFIC SUMMARY FOR A GENERAL AUDIENCE

Many interesting solar systems have been reported in the news, such as the Trappist-1 system which is filled with Earth-like planets. Simulations and models such as those in this paper are used to determine if a planet could be habitable. A habitable zone can be made by varying the parameters of the model to see where the model is habitable, partially habitable, or uninhabitable.

The main model in this paper takes a planet and divides it into a number of latitude bands which can have energy flow between them. Certain parameters, such as how the planet orbits around its star and the angle the planet is tilted at, are varied to build this habitable zone. A result of this paper is if the Earth orbited slightly further away from the Sun then it is likely that it would fall into an ice age similar to what the Earth has experienced in the past. Another result found is that the tilt of the planet can affect how hot or cold it is, and indicates that the current tilt of the Earth gives a cold planet.

Another aspect of this paper's exoplanet research is exomoons orbiting a gas giant such as Jupiter. In certain configurations an exomoon can be heated not only from the host star, but also due to a process called tidal heating. Tidal heating is similar to stretching an elastic band. Stretching and relaxing an elastic band many times can cause the band to warm up. The moon of a gas planet is stretched slightly by unequal forces of gravity as one part of the moon is further away than the other. If the moon's orbit is not circular then the moon is stretched and relaxed, thus heats up in a similar way to the elastic band. Adding tidal heating to the model allows for investigations into how tidal heating can move, or change the shape of, the habitable zone.